Mechanics of Composite Materials, Vol. 41, No. 5, 2005

MODE II DELAMINATION OF A UNIDIRECTIONAL CARBON FIBER/EPOXY COMPOSITE IN FOUR-POINT BEND END-NOTCHED FLEXURE TESTS

E. Zile and V. Tamuzs

Keywords*: four-point bend end-notched flexure, delamination, Mode II, cohesive elements*

Results from an experimental study on the delamination of a unidirectional carbon fiber/epoxy composite by using the four-point bend end-notched flexure (4ENF) test are presented. It was found that the compliance data obtained in load-unload-reload and continuous loading tests were very similar. The R-curves for specimens of different thickness were also found experimentally. These curves showed an appreciable toughening with crack advance, which can be explained by the presence of fiber bridging. The finite-element method with cohesive elements allowing us to model the progressive delamination was used to analyze the 4ENF test.

1. Introduction

The four-point bend end-notched flexure (4ENF) test, introduced recently [1], is increasingly used for determining the Mode II fracture toughness of laminated fiber composites. Unlike the three-point bend end-notched flexure (ENF), in this test, the crack growth is stable under the displacement control. Hence, it is possible to obtain several data points from each specimen, and a complete crack resistance curve (*R*-curve) can be generated from results of just one test. In several studies [2-3], various methods for improving the determination of fracture toughness were investigated. It was recommended in [2] that the compliance in the 4ENF tests be obtained from the slope of the load–deflection plot. This means that the tests must be conducted in a load-unload-reload manner. It was found in [3] that, in the case of non-self-similar crack advance, the compliance calibration method of data reduction is superior to the compliance fitting method.

The goal of the present work was an experimental and numerical investigation of delamination of wedge-precracked unidirectional carbon fiber/epoxy composite beams by using the 4ENF test, since the precracked crack front is thought to represent a naturally occurring crack. The finite-element method with cohesive (interface) elements [4-6], which allow one to model the progressive delamination, was used in the present work.

2. Material and Specimens

We examined a unidirectional Sika CarboDur S 512 carbon fiber/epoxy composite with the elastic modulus in the fiber direction E_1 = 165 GPa, the transverse modulus $E_2 = E_3 = 9$ GPa, the shear modulus G_{12} = 5 GPa, and the Poisson ratio ν_{12} = 0.28. The material was supplied in sheets of thickness ≈1.4 mm, from which strips of necessary length and width were cut and

Institute of Polymer Mechanics, University of Latvia. Russian translated published in Mekhanika Kompozitnykh Materialov, Vol. 41, No. 5, pp. 573-584, September-October, 2005. Original article submitted September 16, 2005.

0191-5665/05/4105-0383

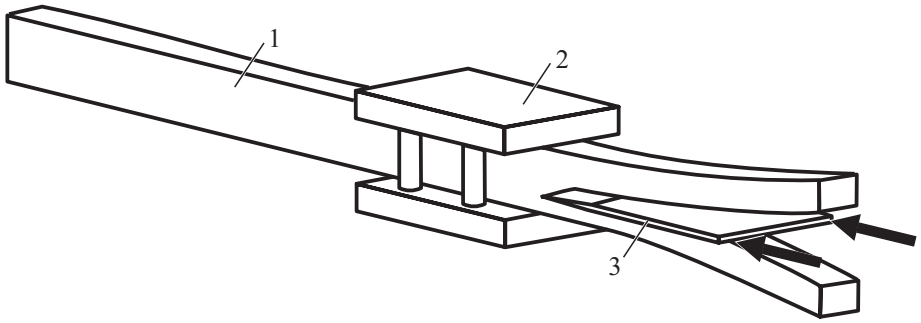

Fig. 1. Wedge precracking technique: 1 — specimen, 2 — clamp, and 3 — wedge.

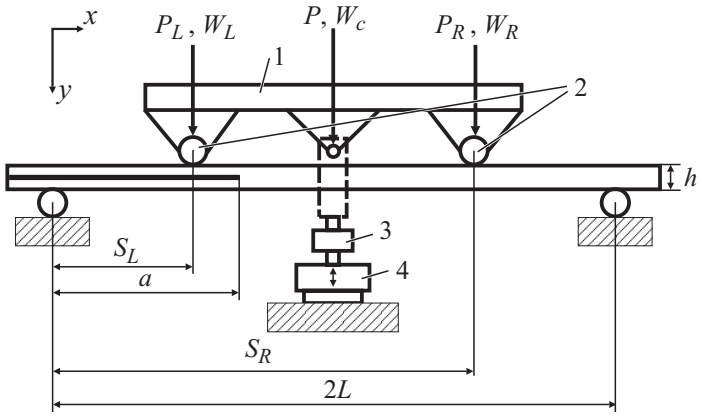

Fig. 2. Schematic of the 4ENF fixture: 1 — loading platen, 2 — loading rollers, 3 — dynamometer, 4 — actuator.

glued together to produce specimens of different thickness. The fibers were oriented along the specimen length. The most suitable adhesive was found to be the “Bison” polyurethane power adhesive.

Prior to gluing, the middle strip was precracked by driving a thin wedge into it (see Fig. 1.). In such a way, high stresses were generated in ready-made specimens when the wedge was closing the clamp, with formation of a damage zone ahead of the tip of the initial crack. Precracking the thin middle strip prior to manufacturing the specimens reduced this effect. The length of the initial crack was 55 mm. A thin Teflon film was placed between surfaces of the initial crack to reduce friction. Specimens with thicknesses of 7.0 mm (five plies and four specimens) and 4.2 mm (three plies and four specimens) were produced. All the specimens were 13.2 mm wide. In order to monitor the position of crack front, the sides of the specimens were painted white, and marks were placed on them at 2-mm intervals.

3. Test Geometry and Beam Theory Analysis

A schematic of the 4ENF fixture is shown in Fig. 2. The loading platen is free to rotate about the axis perpendicular to the specimen length to provide equal forces at the loading pins: $P_L = P_R = P/2$ (pinned configuration). This ensures that the shear force within the inner span is zero and the bending moment is constant. For the pinned configuration, the compliance C is defined as

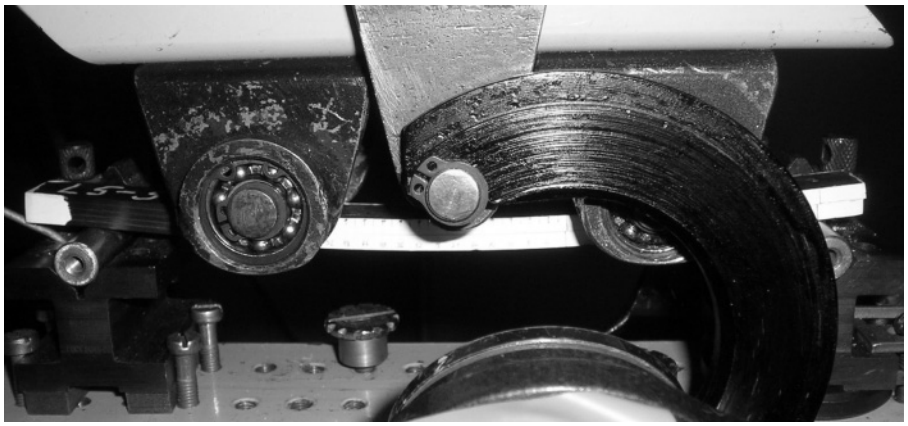

Fig. 3. Photograph of the 4ENF fixture.

$$C = \frac{w_c}{P} = \frac{w_L + w_R}{2P}, \tag{1}$$

where w_c is the deflection at the center of the loading platen, which can be taken equal to the actuator displacement of the testing machine or to the average of two displacements measured by gages located underneath the two loading rollers. The energy release rate is defined in a common way:

$$G = \frac{P^2}{2b}\frac{\partial C}{\partial a}, \tag{2}$$

where b is the specimen width and a is the crack length. For the symmetric configuration ($S_L = L/2$ and $S_R = 3L/2$), the compliance of the system can be expressed as [1]

$$C = \frac{L^3}{48EI}\left(1 + \frac{9a}{L}\right) = C_0 + C_1 a, \tag{3}$$

where I is the second moment of area of the whole cross section of the beam, E is the longitudinal elastic modulus, $C_0 = L^3/48EI$, and $C_1 = 9aL^2/48EI$. Substitution of Eq. (3) in Eq. (2) gives

$$G_{II} = \frac{P^2 C_1}{2b} = \frac{3P^2 L^2}{32EIb}. \tag{4}$$

It was shown in [1] that $\partial G_{II}/\partial a < 0$ under the displacement control. This means that the growth of delamination under the displacement control is stable.

4. Test Procedure

Figure 3 shows a photograph of the 4ENF test fixture used for this study. The following fixture geometry was used: the outer span $2L$ = 160 mm, S_L = 40 mm, and S_R = 120 mm (symmetric configuration). The deformation rate in all the tests was 0.5 mm/min. Two displacement gages were attached to the specimen beneath each loading roller. The initial crack length of 55 mm was chosen because it leaved enough space (15 mm) between the loading roller and the crack tip to avoid any unwanted effects from the compressive stresses of the loading roller [1].

Three specimens of both the thicknesses were loaded, under the displacement control, until the crack advanced slightly. Then the specimens were fully unloaded. The load-unload-reload process was repeated until 6-7 crack propagation

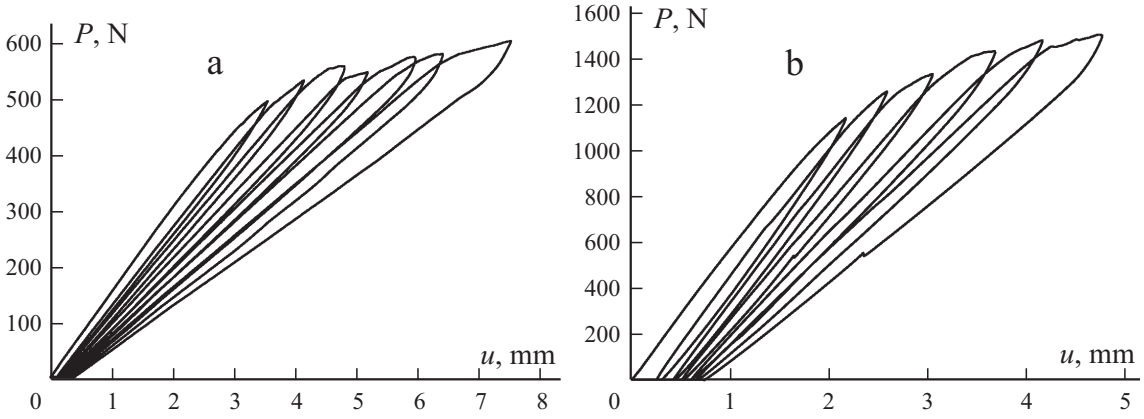

Fig. 4. Typical loading-unloading curves for specimens with thicknesses of 4.2 (a) and 7.0 mm (b).

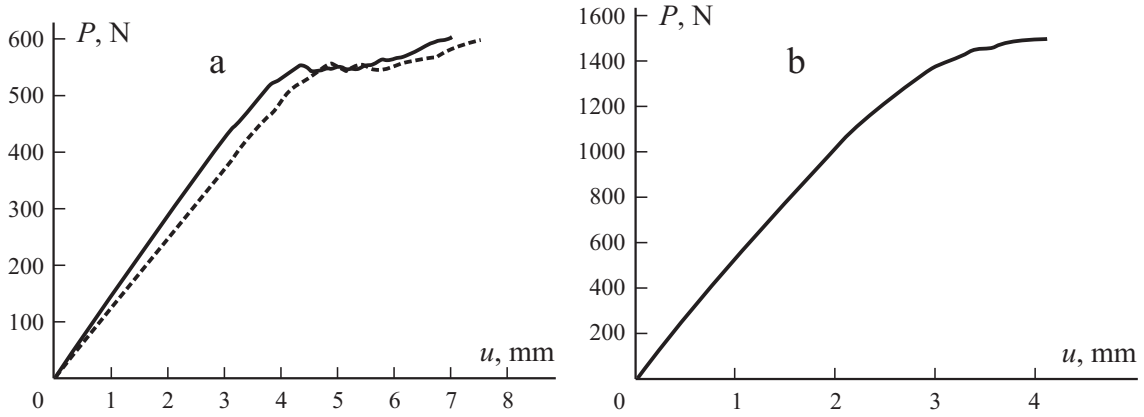

Fig. 5. Continuous loading curve for specimens with thicknesses of 4.2 (a) and 7.0 mm (b). (- - -) — actuator displacement.

events were recorded. During the loading process, the load, the actuator displacement, and readings from the two displacement gages were continuously recorded. A magnifying instrument was used to monitor the crack as it grew. The compliance C at each crack length a was calculated from the slope of load vs. deflection data. The slope of the linear portion of the loading line was used while ignoring any initial nonlinearities due to the take-up of specimens in the load fixture. This yielded a C vs. a curve that could be used to calculate the compliance derivative $\partial C/\partial a$, which was needed to compute G_c [Eq. (2)]. When using Eq. (2), any errors due to uncertainties in the geometric or material properties are avoided.

One specimen from both the thicknesses was loaded continuously. The compliance during this test was defined simply as the critical displacement divided by the critical load.

5. Experimental Results

The typical loading/unloading curves P–u, plotted against the average of two readings from the displacement gages for the 4.2 and 7.0-mm thick specimens, are shown in Fig. 4. The corresponding curves for the continuous loading are seen in Fig. 5. Figure 5a also shows the loading curve plotted against the actuator displacement, which is larger than the average measurements by the two displacement gages because of the additional deflection in the loading system. The crack growth was in-

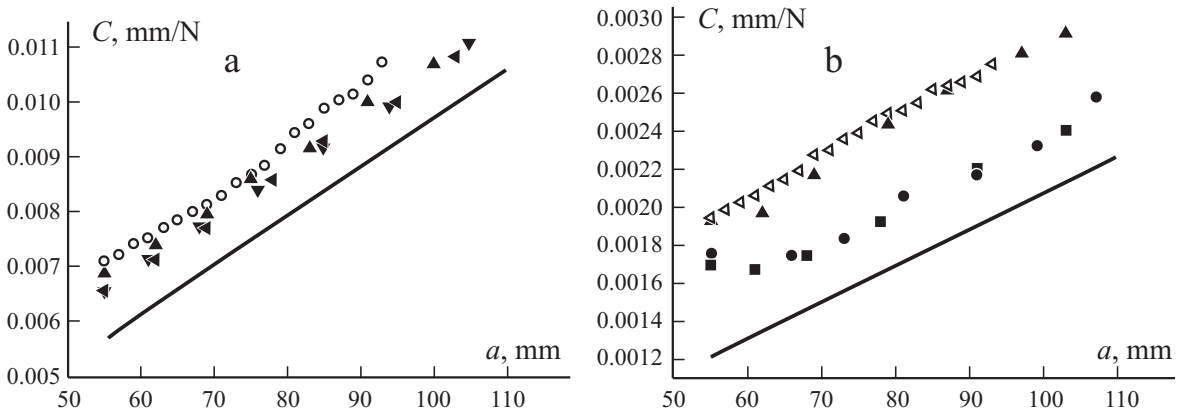

Fig. 6. Experimental compliance of specimens with thicknesses of 4.2 (a) and 7.0 mm (b). Solid line — beam-theory prediction. Open symbols — results from the continuous loading test. Various symbols indicate different specimens.

TABLE 1. Average Values of Compliance Derivatives $\partial C/\partial a$, N^{-1}

Specimen thickness, mm	Experiment	Beam theory
4.2	$8.96 \cdot 10^{-5}$	$8.92 \cdot 10^{-5}$
7.0	$1.80 \cdot 10^{-5}$	$1.90 \cdot 10^{-5}$

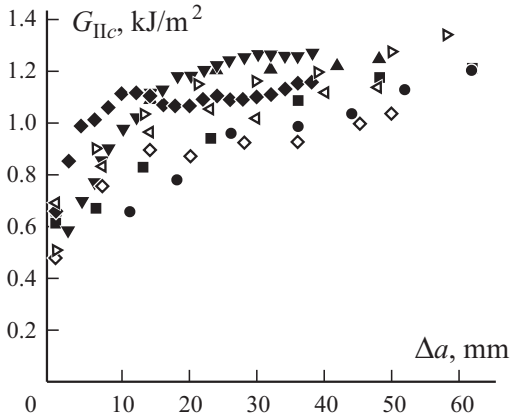

Fig. 7. *R*-curves from the 4ENF tests. Open symbols — results from specimens with a thickness of 4.2 mm. Closed symbols — results from specimens with a thickness of 7.0 mm. Various symbols indicate different specimens.

variably stable during the test. The readings from the displacement gages were used to calculate the compliances, which are shown in Fig. 6.

What is important, however, is not the compliance curve itself but its derivative $\partial C/\partial a$. The experimental compliance versus crack length data was fit with a straight line, whose slope $\partial C/\partial a$ is constant. This method of data reduction is called the "compliance fitting."

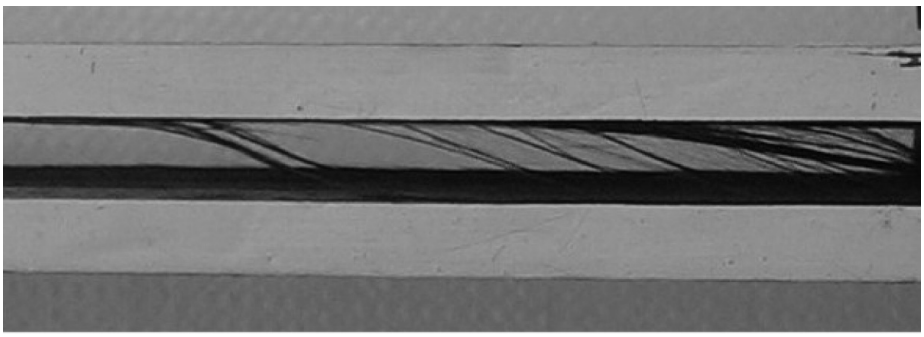

Fig. 8. Bridging zone.

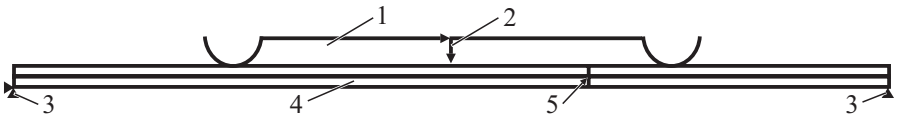

Fig. 9. Geometry of 4ENF tests for FEA: 1 — loading platen, 2 — load, 3 — supports, 4 — cohesive elements, and 5 — initial crack tip.

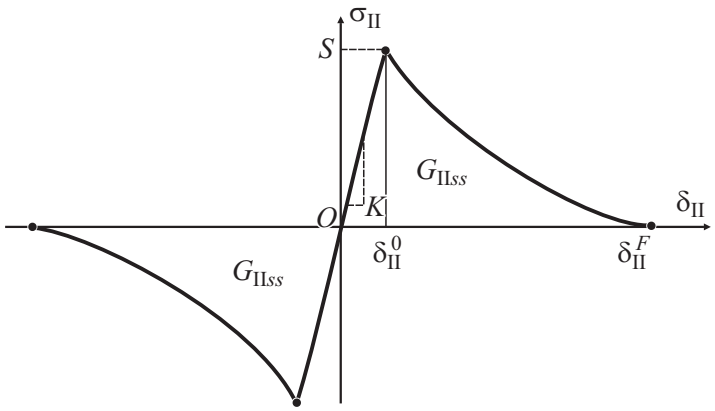

Fig. 10. Traction–separation relationship for the cohesive elements.

The average values of $\partial C/\partial a$ from all the tests and the compliances following from the beam theory are shown in Table 1. As is seen, all the experimental compliances are larger than that predicted by the beam theory (possibly due to shear deformations in the specimens), but the derivatives agree well. The compliance curves and the derivatives $\partial C/\partial a$ obtained from the continuous loading test are close to the curves and $\partial C/\partial a$ obtained from the load-unload-reload test.

The critical energy release rate G_{IIc} was calculated from Eq. (2). The *R*-curves obtained are shown in Fig. 7. Contrary to the results of previous researchers [1-2], our *R*-curves show appreciable toughening with crack advance. The average initiation value G_{IIo} is 0.61 kJ/m^2, and the average steady-state value G_{IIss} is 1.16 kJ/m^2. An examination of the specimens after the tests revealed the presence of fiber bridging (Fig. 8), which can explain the toughening effect observed.

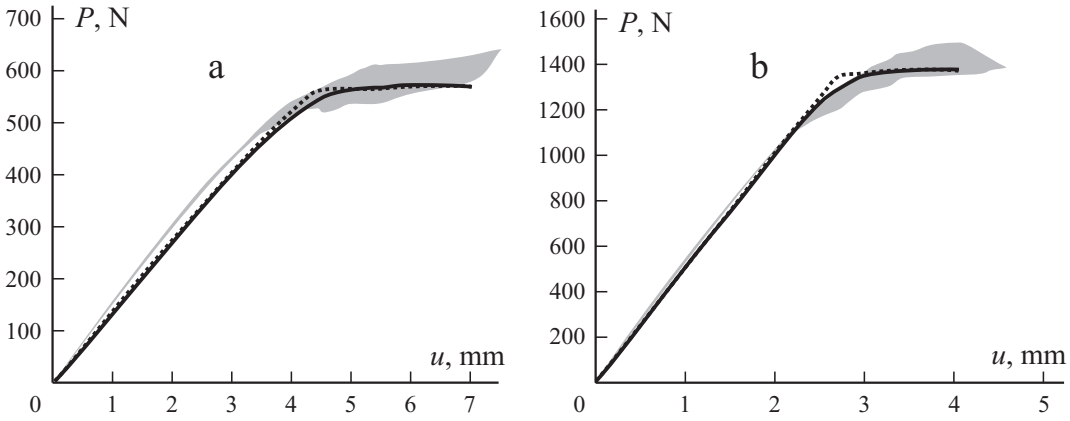

Fig. 11. FEA results for specimens with thicknesses of 4.2 (a) and 7.0 mm (b). The shaded area — experimental results; (——) and (- - -) — exponential and linear softening models, respectively.

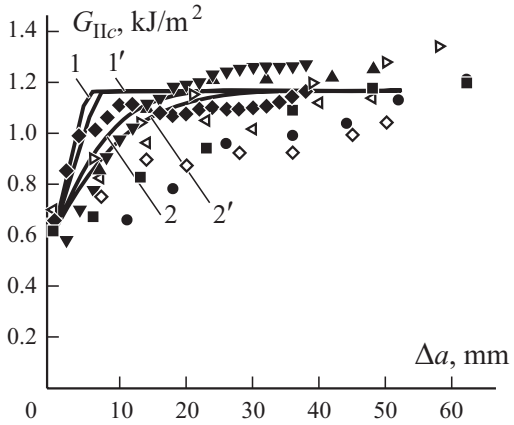

Fig. 12. *R*-curves predicted by the linear (1, 1′) and exponential (2, 2′) softening models for specimens with thicknesses of 4.2 (1, 2; open symbols) and 7.0 mm (1′, 2′; closed symbols).

6. Numerical Simulation by Using the Finite-Element Method

A two-dimensional plain-strain finite-element analysis (FEA) of the 4ENF test was conducted by using ABAQUS version 6.5. The delamination was simulated with the aid of cohesive elements (ABAQUS naming convention COH2D4) embedded along the potential delamination line (see Fig. 9). The loading platen with rollers was modeled as a rigid analytical surface. The interaction between the specimen and the loading rollers was provided by using contact algorithms incorporated into the code. Only the delamination within the loading rollers was considered.

The crack propagation was simulated by introducing a softening traction–separation relationship σ_{II}–δ_{II} for the cohesive elements (see Fig. 10). For the Mode II loading, the separation δ_{II} is the relative sliding of crack surfaces, and tractions are the shear stresses acting on the crack surfaces. After the interfacial shear tractions have reached the interlaminar shear strength *S*, they decrease according to the softening model and vanish when complete decohesion occurs. The fracture mechanics is introduced indirectly, by relating the area under the traction–separation curve to the steady-state energy release rate G_{IIss}. The precise value of the shear strength *S* has little effect on the computed response. It should be a good estimate of the actual shear

strength. The initial stiffness K should be high enough to simulate the initially very stiff interface, but very high K values cause convergence problems during solution. The simulation was performed by using two different — linear (tractions vanished at $\delta_{II}^{F} = 0.08$ mm) and exponential (tractions vanished at $\delta_{II}^{F} = 0.25$ mm) — softening models. A comparison of the predicted and measured load–displacement and R-curves are presented in Figs. 11 and 12. It can be seen that the damage model has a negligible effect on the load level during the steady-state crack propagation. A sufficiently good agreement with the experimental data is observed. The shape of the predicted load–displacement and R-curves obtained by using the exponential damage model is more similar to the shape of the experimental curves than that of the curves obtained by using the linear damage model.

Conclusions

1. The compliance data and the derivatives $\partial C/\partial a$ obtained from the continuous loading test are close to those obtained from the load-unload-reload test. This means that both the loading techniques can be used to obtain the critical energy release rate G_{IIc}.

2. The experimental R-curves show an appreciable toughening with crack advance. This fact can be explained by the presence of fiber bridging, which was found during inspection of the specimens after the tests (Fig. 8).

3. A finite-element analysis with cohesive elements reveals a good agreement between the numerical and experimental load–displacement curves and R-curves.

Acknowledgements. The work was supported by the European Social Fund.

REFERENCES

1. R. H. Martin and B. D. Davidson, “Mode II fracture toughness evaluation using four-point bend end-notched flexure test,” Plastics, Rubber, Compos., **28**, 8, 401-406 (1999).
2. C. Schuecker and B. D. Davidson, “Evaluation of the accuracy of the four-point bend end-notched flexure test for mode II delamination toughness determination,” Compos. Sci. Technol., **60**, 2137-2146 (2000).
3. A. J. Vinciquerra and B. D. Davidson, “Effect of crack length measurement technique and data reduction procedures on the perceived toughness from four-point bend end-notched flexure tests,” J. Reinf. Plastics Compos., **23**, No. 10, 1051-1062 (2004).
4. Y. Mi, M. A. Crisfield, G. A. O. Davies, and H. B. Hellweg, “Progressive delamination using interface elements,” J. Compos. Mater., **32**, No. 14, 1246-1272 (1998).
5. P. P. Camanho and C. G. Davila, “Mixed-mode decohesion finite elements for the simulation of delamination in composite materials,” NASA/TM-2002-211737.
6. ABAQUS Version 6.5 Documentation, Hibbitt, Karlsson & Sorensen, Pawtucket, RI.